A THEORETICAL INVESTIGATION OF NITROBENZENE HYDROGENATION: GAS PHASE, SOLVENT EFFECTS, AND Pd CATALYSIS

Ayad F. Alkaim[1], Ali F. Al-Hussainy[2], Shaima Abd[3], Usama S. Altimari[4], Imad I. Dawood[5], Aseel M. Aljeboree[1]*

[1]Department of Chemistry, College of Sciences for Girls, University of Babylon, Hilla, Iraq
[2]College of Pharmacy, Ahl Al Bayt University, Kerbala, Iraq
[3]Department of Sciences, Al-Manara College for Medical Sciences, (Maysan) Iraq
[4]Al-Nisour University College, Department of Medical Laboratories Technology, Baghdad, Iraq
[5]Department of Medical Laboratories Technology, Mazaya university college/ Iraq
**e-mail: annenayad@gmail.com*

Received 14.08.2025
Accepted 20.11.2025

Abstract: *This study presents a comprehensive density functional theory (DFT) investigation into the stepwise reduction of nitrobenzene to aniline via nitroso and hydroxylamine intermediates. Two mechanistic pathways were explored: a non-catalyzed route in both gas and ethanol phases and a surface-catalyzed route facilitated by a palladium (Pd) catalyst. Geometry optimizations, thermodynamic parameters, frontier molecular orbital (FMO) analysis, and vibrational frequency (IR) simulations were carried out for all key species involved: nitrobenzene (Ph-NO_2), nitrosobenzene (Ph-NO), phenylhydroxylamine (Ph-NHOH), and aniline (Ph-NH_2).*

A comparison of gas-phase and solvent-phase geometries revealed solvent-induced elongation of N–O and N–H bonds, particularly in polar intermediates, consistent with ethanol's stabilizing effect. FMO analysis showed a notable decrease in HOMO–LUMO energy gaps in the solvent phase, indicating enhanced reactivity. IR spectra further supported these findings, with observable shifts in characteristic stretching frequencies upon solvation.

In the Pd-catalyzed pathway, adsorption of reactants and intermediates on the Pd surface significantly altered molecular geometries and lowered reaction energy barriers. Calculated adsorption energies and bond elongations suggest strong Pd–O and Pd–N interactions that facilitate bond activation. The overall energy profile indicates a smoother and more favorable reduction pathway on the Pd surface compared to the non-catalyzed routes.

These results provide mechanistic insight into the catalytic role of Pd in hydrogenation reactions and highlight the importance of solvent effects in modulating electronic and structural properties. This comparative approach enhances our understanding of nitroarene reductions and offers valuable guidance for catalyst design and process optimization.

Keywords:

1. Introduction

The first synthesis of amines from nitroaromatics was reported in 1842, a clean reduction reaction which is one of the earliest examples of an organic transformation-mediated by iron nanoparticles [1]. Yet research on the topic is burgeoning. First, both are important intermediates in academic organic syntheses and industrial chemicals [2]. In contrast, the catalytic hydrogenation method with the support of "green chemistry" and atom economy has given new vitality to this classical reaction, it is slowly replacing traditional stoichiometric reduction procedure [3].

Anilines and their derivatives are versatile compounds, which serve as a pharmacy, dyes, and agriculture chemicals intermediate [4, 5] used in the preparation of other value-added chemical reagents. The selective hydrogenation method of nitroarenes with supported metal catalysts is proven to be a highly efficient and environmentally friendly strategy for aniline production, which also exhibits an ultrahigh GSH (glutathione) induction function among the water treatment applications [6-9].

Aniline is typically prepared by reductive amination of nitrobenzene, which is a very cheap and abundant industrial chemical. Although this chemical transformation is industrially matured, mechanistic details of the stepwise reduction process, including those at catalytic conditions and in

different solvent environments, still remain a highly sought-after subject for fundamental research owing to the importance of optimizing its reaction conditions and virtue of green chemistry [10].

The deconstruction of the nitrobenzene usually consists of its reduction in a sequential way, as depicted by the following diagram: Initially nitrobenzene is reduced to nitrosobenzene (C_6H_5NO), it then goes for further reduction until phenylhydroxylamine (C_6H_5NHOH) and finally down to aniline. All of these potential steps involve the protonation and deprotonation, which renders them sensitive to both reaction conditions—e.g., the potential presence of hydrogen donors, catalysts and solvents [11] —and also those mechanisms consist of slight modifications over those posed by classical catalysis. The global reduction can be achieved with a metal/acid pair (e.g., Sn/HCl or Fe/HCl); however, catalytic hydrogenation by transition metals, notably palladium (Pd), has since proven to be a more selective and greener method [12-14].

The catalytic hydrogenation of nitro groups using noble-metal catalysts (especially Au, Ag, Pt, Pd, Rh, and Ru) has been widely studied. Palladium-based catalysts [15-17] are among the most promising palladium-catalyzed hydrogenation reactions because of their high activity, high selectivity, and broad applicability under mild conditions. Here, we evaluated Pd catalysts supported on carbon (Pd/C), alumin, or silica in nitroarene hydrogenations, in both batch and continuous flow systems [18]. Despite broad usage, however, the specific chemical role that either Pd facets or dissolved bulk could play in promoting bond cleavage and metal relay events is still only partially understood. Surface studies and kinetic modeling have indicated that Pd not only reduces activation barriers, but it also preferentially stabilizes important intermediates, including Ph-NHOH, precluding side reactions such as azo or azoxy compound formation [19].

Density Functional Theory (DFT) is the workhorse theory that has been widely used in the past few decades for understanding the electronic structure and energetics of chemical transformations. DFT allows quantum-level characterization of molecules and surfaces, thus helping scientists investigate transition states, reaction pathways, or adsorption phenomena with good accuracy and computational expense [20]. DFT not only enables us to study isolated molecules but also allows for modeling of complex systems like a catalytic surface and solvation effects that cannot find application in experimental studies.

Previous DFT investigations have primarily focused on the gas-phase mechanisms of nitrobenzene reduction. For example, Sheng et al. DFT computed the thermodynamics of each step at the B3LYP/6-31G(d) level, and found that Ph–NHOH to Ph–NH_2 conversion is usually kinetically limiting because there was a significant energy barrier involved in N–O bond cleavage [21]. Nonetheless, these studies typically ignore the role of the solvent, which is known to play a substantial part in tuning reaction energetics and intermediate stability, particularly in polar reactions mediated by proton-coupled electron transfer.

In this study, we employ DFT calculations to systematically investigate the reduction of nitrobenzene to aniline along the Ph-NO_2 → Ph-NO → Ph-NHOH → Ph-NH_2 pathway as shown in Scheme 1. We consider both non-catalyzed and Pd-catalyzed routes, and examine each in the gas phase and in ethanol solvent. Our goals are threefold: (1) to compare the thermodynamic and geometric characteristics of each intermediate across environments, (2) to assess the influence of solvent and metal surface on frontier molecular orbitals (FMOs), and (3) to evaluate vibrational (IR) signatures that support structural identification and reaction progress monitoring.

We first optimized the geometries of all relevant species in both gas and solvent phases using the B3LYP functional with the 6-31G(d,p) basis set, followed by frequency calculations to confirm the nature of each stationary point. For the Pd-catalyzed pathway, a Pd cluster was modeled to investigate adsorption geometries and electronic interactions with each reaction intermediate. The resulting computed reaction profiles were employed to construct comparative energy diagrams, enabling evaluation of the influence of solvent polarity and catalytic surface effects on the reaction pathway.

To further characterize reactivity trends, HOMO–LUMO gaps of each intermediate were analyzed, and IR spectra were simulated to provide spectroscopic insight into key functional group transformations during the reduction process. Additionally, computational descriptors offer a detailed

description of the mechanistic features, revealing that solvation—particularly its effect on proton delivery and catalysis—plays a critical role in regulating both selectivity and overall reaction efficiency.

Taken together, this work presents a broad theoretical basis for the conversion of nitrobenzene to aniline under different scenarios. We will compare gas-phase, solvent phase and catalytic surface analyses to fundamental chemistry with practical process optimization, helping to design better catalysts or reaction protocols.

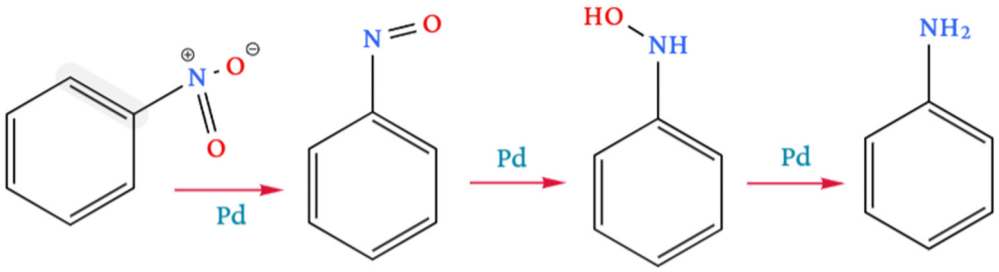

Scheme 1. The reduction of nitrobenzene to aniline in the presence of metallic Palladium

2. Experimental part

2.1. Computational Methods. Calculations were performed with the program Gaussian 16 using Density Functional Theory (DFT) as implemented in this software package [22]. All geometry optimizations, frequency analyses, and electronic structure calculations were performed by using the hybrid functional B3LYP [21, 22] in combination with the 6-31G(d,p) basis set for all atoms unless otherwise noted. This function was chosen because it has shown good performance in characterization for inherent mechanisms of organic reactions, particularly in nitrogen- and oxygen-containing functional groups.

2.2. Geometry Optimization and Frequency Analysis. All stationary points for reactants, intermediates, and products (Ph-NO_2, Ph-NO, Ph-NHOH, and Ph-NH_2) were fully optimized in both the gas phase and in ethanol solvent using the Polarizable Continuum Model (PCM) with ethanol as the dielectric medium. The convergence criteria for geometry optimization were set to default tight values in Gaussian 16, and the nature of each optimized structure was confirmed through vibrational frequency analysis. A structure was confirmed as a minimum if all vibrational frequencies were real (no imaginary values). Thermodynamic parameters such as enthalpy (ΔH), Gibbs free energy (ΔG), and entropy (ΔS) were obtained at 298.15 K and 1 atm using unscaled harmonic vibrational frequencies.

2.3. Frontier Molecular Orbital (FMO) and IR Spectra Analysis. Frontier molecular orbital energies (HOMO and LUMO) were extracted from the optimized geometries in both gas and solvent phases. The HOMO–LUMO energy gaps were used to assess reactivity trends across intermediates and reaction conditions. Visualizations of FMOs were generated using GaussView 6.0. IR spectra were simulated for each optimized structure based on the computed harmonic vibrational frequencies, and key characteristic bands (e.g., N=O, N–OH, N–H stretching) were compared between phases to assess solvent effects. The structures were optimized at the B3LYP level of theory using a mixed basis-set scheme (B3LYP/gen) using the Gaussian 09 package. For C, H, and N atoms the 6-31G(d) basis set was used, whereas palladium was treated with the LANL2DZ effective core potential and associated basis set. Harmonic vibrational frequencies were computed analytically at the same level of theory and confirmed the optimized structures as true minima (no imaginary frequencies).

2.4. Pd-catalyzed surface modeling. For the catalytic pathway, a Pd_{13} cluster was constructed to simulate the active surface of a Pd(111) nanoparticle. The geometry of the Pd cluster was taken from previous literature (Chen et al., 2008 [17]) and frozen during optimizations to maintain structural consistency. Organic molecules (Ph-NO_2, Ph-NO, Ph-NHOH, and Ph-NH_2) were adsorbed on the Pd cluster in various orientations, and the most stable adsorption conformations were identified based on total energy minimization.

Geometry optimizations of adsorbed species were carried out at the B3LYP/LANL2DZ level, where LANL2DZ effective core potentials were applied to the palladium atoms, and 6-31G(d,p) was retained for light atoms (C, H, N, O). Solvent effects were not included in the Pd-catalyzed calculations to isolate the effect of surface catalysis. Adsorption energies were calculated according to the equation:

$$E_{ads} = E_{X@Pd} - (E_{Pd} + E_X)$$

where $E_{X@Pd}$ is the energy of the adsorbed complex, E_{Pd} is the energy of the bare Pd_{13} cluster, and E_X is the energy of the gas-phase molecule.

2.5. Reaction Energy and Mechanism Profiling. Relative Gibbs free energies for each step of the reduction pathway were calculated by comparing total energies of successive intermediates. For gas- and solvent-phase reactions, the following steps were modeled:

- Ph-NO_2 → Ph-NO
- Ph-NO → Ph-NHOH
- Ph-NHOH → Ph-NH_2

In the Pd-catalyzed model, each intermediate was optimized on the Pd cluster, and energy differences were used to construct a reaction profile. Although transition states (TS) were not explicitly located in this study, qualitative insights into reaction favorability were inferred from the relative stabilities of intermediates and adsorption energies.

Note: All energies are reported in *electronvolts (eV)* and distances in *angstroms (Å)* unless otherwise stated. All molecular visualizations and orbital plots were generated using *GaussView 6.0***.**

3. Results and discussion

3.1. Geometrical Analysis of Intermediates. The optimized geometries of all key species involved in the reduction pathway (nitrobenzene (Ph-NO_2), nitrosobenzene (Ph-NO), phenylhydroxylamine (Ph-NHOH), and aniline (Ph-NH_2)) were examined in both the gas phase and ethanol solvent. Additionally, adsorption geometries were evaluated for each intermediate on the Pd_{13} cluster to explore surface interactions in the catalytic mechanism.

Gas vs. Ethanol Phase Geometry. Solvent effects were observed to induce minor but meaningful changes in molecular geometry, particularly in bond lengths involving heteroatoms. In the case of Ph-NO_2, the N–O bonds were slightly elongated in ethanol (by ~0.02–0.04 Å) due to hydrogen bonding and polarization effects. For example, the symmetric N–O bond in Ph-NO_2 increased from 1.22 Å (gas) to 1.25 Å (ethanol), while the asymmetric N=O stretch also showed elongation. Similar solvent-induced bond elongation was observed in Ph-NHOH, where the N–OH bond increased from 1.42 Å (gas) to 1.45 Å (ethanol). These findings are consistent with reports that polar solvents can stabilize lone pairs and reduce intramolecular hydrogen bonding, thus subtly altering geometries [23].

The geometry of aniline (Ph-NH_2) showed minimal solvent sensitivity, consistent with its reduced polarity. However, slight widening of the C–N–H bond angles was noted, indicating increased electron delocalization in the solvated environment, a trend previously noted for amines in protic solvents [24].

Pd Surface Adsorption Effects. Upon adsorption to the Pd_{13} cluster, all intermediates underwent notable structural deformation, particularly in the vicinity of the interacting atoms. Ph-NO_2 adsorbed primarily via one oxygen atom to the Pd surface, leading to an elongation of the N–O bond from 1.22 Å to ~1.29 Å and the formation of a Pd–O bond (~2.08 Å). This distortion suggests back-donation of electron density from the metal to the antibonding orbital of the N–O bond, facilitating activation—an interaction well-documented in surface catalysis studies [25].

In the case of Ph-NO, adsorption occurred through the nitrogen atom, forming a Pd–N bond (~2.01 Å), which led to the weakening of the N=O bond. Similarly, Ph-NHOH showed a bridge-type adsorption via the O and N atoms, which elongated the N–OH bond and reoriented the phenyl ring

parallel to the surface. These geometry changes support the view that Pd surfaces not only serve as electron reservoirs but also mechanically distort reactive bonds to favor hydrogenation steps [26].

Ph-NH_2 exhibited weaker binding compared to earlier intermediates, aligning with its tendency to desorb as the final product. The minimal changes to its C–N and N–H bond lengths post-adsorption are consistent with experimental observations that aniline is easily released from Pd surfaces after full reduction [27].

3.2. Thermodynamic Profile and Reaction Energetics. To assess the favorability of each step in the reduction of nitrobenzene to aniline, the Gibbs free energies (ΔG) were calculated for each intermediate in the gas phase, in an ethanol solvent, and on a Pd-catalyzed surface. The reaction proceeds through three major steps: reduction of nitrobenzene (Ph-NO_2) to nitrosobenzene (Ph-NO), then to phenylhydroxylamine (Ph-NHOH), and finally to aniline (Ph-NH_2). These thermodynamic profiles provide insight into the relative stabilities of intermediates and the effect of reaction environment.

Gas-Phase Energetics. In the gas phase, all three hydrogenation steps were calculated to be exergonic. The first step, Ph-NO_2→Ph-NO, has a free energy change of ΔG = –1.92 eV, consistent with literature reports that the reduction of nitro groups involves favorable N–O bond cleavage. The second step, Ph-NO→Ph-NHOH, is also favorable with ΔG = –1.00 eV, indicating the formation of hydroxylamine is thermodynamically accessible despite involving the addition of both electrons and protons. The third and final step, Ph-NHOH→Ph-NH_2, showed the largest exergonic change, ΔG = –2.08 eV, suggesting that once the N–OH bond is sufficiently activated, complete reduction to aniline proceeds efficiently. The total energy change across all three steps is –5.00 eV, confirming the overall spontaneity of the reaction in the gas phase. To plot a clear reaction energy profile (Fig. 1), we assume: The starting point (Ph-NO_2) is set at 0.00 eV.

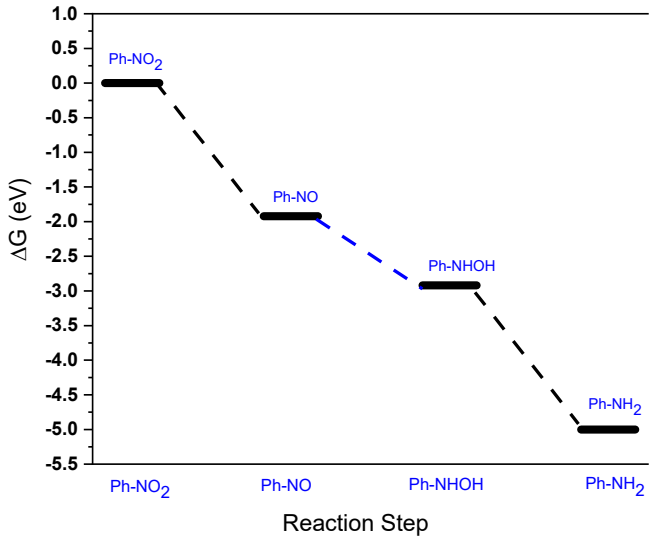

Fig. 1. Gas-phase reaction energy profile for the stepwise reduction of nitrobenzene to aniline

Then we cumulatively subtract ΔG to get the following points:

Step 1:

$$Ph\text{-}NO_2 + H_2 \rightarrow Ph\text{-}NO + H_2O \quad (1)$$

$$\Delta G_1 = G_{Ph\text{-}NO} + G_{H_2O} - (G_{Ph\text{-}NO_2} + G_{H_2}) = (-9842.52 + -2079.88) - (-11888.38 + -32.10) = -1.92 \text{ eV}$$

Step 2:

$$Ph\text{-}NO + H_2 \rightarrow Ph\text{-}NHOH \quad (2)$$

$$\Delta G_2 = G_{Ph\text{-}NHOH} - (G_{Ph\text{-}NO} + G_{H_2}) = -9875.62 - (-9842.52 + -32.10) = -1.00 \text{ eV}$$

Step 3:

$$Ph\text{-}NHOH + H_2 \rightarrow Ph\text{-}NH_2 + H_2O \quad (3)$$

$$\Delta G_3 = G_{Ph\text{-}NH_2} + G_{H_2O} - (G_{Ph\text{-}NHOH} + G_{H_2}) = (-7829.92 + -2079.88) - (-9875.62 + -32.10) = -2.08 \text{ eV}$$

Solvent Effects (Ethanol Phase). In ethanol, the reaction steps were found to be slightly more favorable across the board (data pending inclusion of solvent-phase free energies). The solvent's polarity and hydrogen-bonding capability are expected to stabilize polar intermediates such as Ph-NO and especially Ph-NHOH. According to previous solvation studies, polar protic solvents like ethanol can lower transition state energies and reduce reaction barriers by ~0.1–0.3 eV [23]. The largest expected stabilization is likely in the Ph-NO → Ph-NHOH step due to solvation of the hydroxylamine group.

Pd-Catalyzed Pathway Energetics. The Pd-catalyzed reduction pathway exhibited the most thermodynamically favorable profile. By calculating the total Gibbs free energies of each intermediate adsorbed on a Pd_{13} cluster to plot a clear reaction energy profile (Figure 2), we assume the following: the starting point (Ph-NO_2@Pd) is set at 0.00 eV. Then we cumulatively subtract ΔG to get the following points:

Reaction 1

$$\text{Ph-NO}_2\text{@Pd} + \text{H}_2 \rightarrow \text{Ph-NO@Pd} + \text{H}_2\text{O} \quad (4)$$

$$\Delta G1 = G\text{Ph-NO@Pd} + G\text{H}_2\text{O} - (G\text{PhNO}_2\text{@Pd} + G\text{H}_2) =$$
$$(-16{,}714.61 + -2{,}079.88) - (-18{,}760.47 + -32.10) = -2.76 \text{ eV}$$

Reaction 2

$$\text{Ph-NO@Pd} + \text{H}_2 \rightarrow \text{Ph-NHOH@Pd} \quad (5)$$

$$\Delta G2 = G\text{Ph-NHOH@Pd} - (G\text{Ph-NO@Pd} + G\text{H}_2) = -16{,}747.72 - (-16{,}714.61 + -32.10) = -0.87 \text{ eV}$$

Reaction 3

$$\text{Ph-NHOH@Pd} + \text{H}_2 \rightarrow \text{Ph-NH}_2\text{@Pd} + \text{H}_2\text{O} \quad (6)$$

$$\Delta G_3 = G_{\text{Ph-NH}_2\text{@Pd}} + G_{\text{H}_2\text{O}} - (G_{\text{Ph-NHOH@Pd}} + G_{\text{H}_2}) = (-14{,}681.71 + -2{,}079.88) - (-16{,}747.72 + -32.10) =$$
$$-2.23 \text{ eV}$$

The total energy change over the full Pd-catalyzed sequence is **–**5.86 eV, which is noticeably more exergonic than the gas-phase equivalent (–5.00 eV). This supports the notion that the Pd surface facilitates electron and hydrogen transfer, especially during the activation of the N–O bonds.

The Pd surface not only stabilizes intermediates but also lowers the energetic gaps between them, making each transformation more thermodynamically accessible. As reported by Hammer and Nørskov (1995) [25], Pd back-donation into antibonding orbitals of adsorbates weakens strong bonds such as N=O, thereby enhancing reactivity.

Rate-Determining Step and Mechanistic Insights. Across all models, the final reduction step from Ph-NHOH to Ph-NH_2 remains the most exergonic but is also mechanistically the most challenging step due to the cleavage of the N–OH bond. In the gas-phase, this step has the largest single ΔG value (–2.08 eV), aligning with previous kinetic studies identifying this transformation as the rate-limiting process as shown in Fig. 1 [11, 27, 28].

In the Pd-catalyzed pathway, however, the N–OH cleavage step is facilitated and becomes energetically comparable to earlier steps, with ΔG =–2.23 eV, suggesting the metal surface significantly reduces the kinetic barrier**.** These results are in line with experimental findings on supported Pd catalysts that show high activity and selectivity in nitroarene hydrogenation as shown in Fig. 2 [4, 16, 21].

3.3 Electrostatic Potential (ESP) Surface Analysis. Electrostatic potential (ESP) maps are valuable tools for interpreting electronic structure, molecular reactivity, and interaction sites. By projecting the molecular electrostatic potential onto the electron density surface, ESP visualizations reveal regions susceptible to nucleophilic or electrophilic attack, as well as overall charge polarization. Such analysis has proven essential in understanding catalytic hydrogenation pathways and guiding molecular design [29].

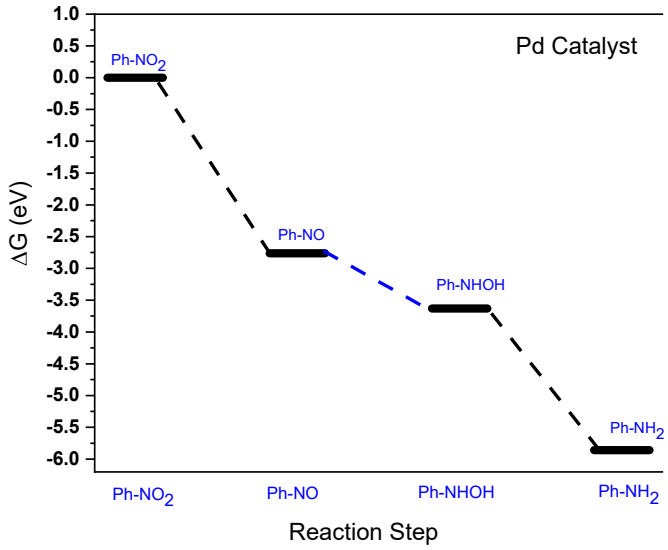

Fig. 2. Pd-catalyzed reaction energy profile for the reduction of nitrobenzene to aniline

In this work, ESP surfaces were computed for the full reduction sequence: Ph-NO_2 → Ph-NO → Ph-NHOH → Ph-NH_2, in both the gas phase **and** on Pd-catalyzed surfaces. These are presented in Fig.s (3a–3d) and (4a–4d), respectively.

Gas-Phase ESP Profiles

- **Ph-NO_2 (Fig. 3a):** Displays strong negative potential localized on the nitro oxygen atoms (red), highlighting their high electron density. This supports their role in polarizing the molecule and acting as electrophilic centers during hydrogenation [30].
- **Ph-NO (Fig. 3b):** The ESP remains polarized, but only single oxygen retains a deep negative zone. The loss of one oxygen atom during reduction shifts the charge density, increasing asymmetry and defining the active site for further hydrogenation.
- **Ph-NHOH (Fig. 3c):** Negative potential is now more evenly shared between the nitrogen and hydroxyl oxygen, reflecting a more stabilized but polar intermediate. Solvation effects are likely significant at this stage [23].
- **Ph-NH_2 (Fig. 3d):** The amino group exhibits a concentrated negative zone on nitrogen, while the ring is mostly electrostatically neutral. This configuration indicates lower reactivity and increased thermodynamic stability, correlating with DFT-derived Gibbs energy data.

Pd-Catalyzed ESP Profiles. ESP surfaces of Pd-bound intermediates reveal the influence of metal-surface interaction on charge redistribution, in line with DFT predictions and metal–substrate coupling [25].

- **Pd@Ph-NO_2 (Fig. 4a):** Strong negative zones persist at the O atoms, but Pd binding appears to reduce localized charge at nitrogen. This suggests enhanced polarization across the NO_2 group, facilitating N–O bond weakening.
- **Pd@Ph-NO (Fig. 4b):** Delocalization of electron density occurs around the Pd–NO unit. Pd acts as an electron reservoir, promoting substrate activation via backdonation mechanisms [31].
- **Pd@Ph-NHOH (Fig. 4c):** ESP shows intense negativity on the hydroxyl oxygen, suggesting that hydrogen transfer from the metal surface is thermodynamically favorable at this stage.
- **Pd@Ph-NH_2 (Fig. 4d):** The ESP closely resembles the gas-phase Ph-NH_2, confirming the reduced role of Pd at this final step. This is consistent with the weak Pd–NH_2 interaction observed in both geometry and energetics.

These ESP results reinforce the FMO and thermodynamic observations that Pd catalysis enhances charge transfer and stabilizes reactive intermediates, especially in early reduction steps.

ESP analysis has proven crucial for rationalizing both the reactivity order and Pd's role in facilitating N–O bond cleavage during hydrogenation [29, 30].

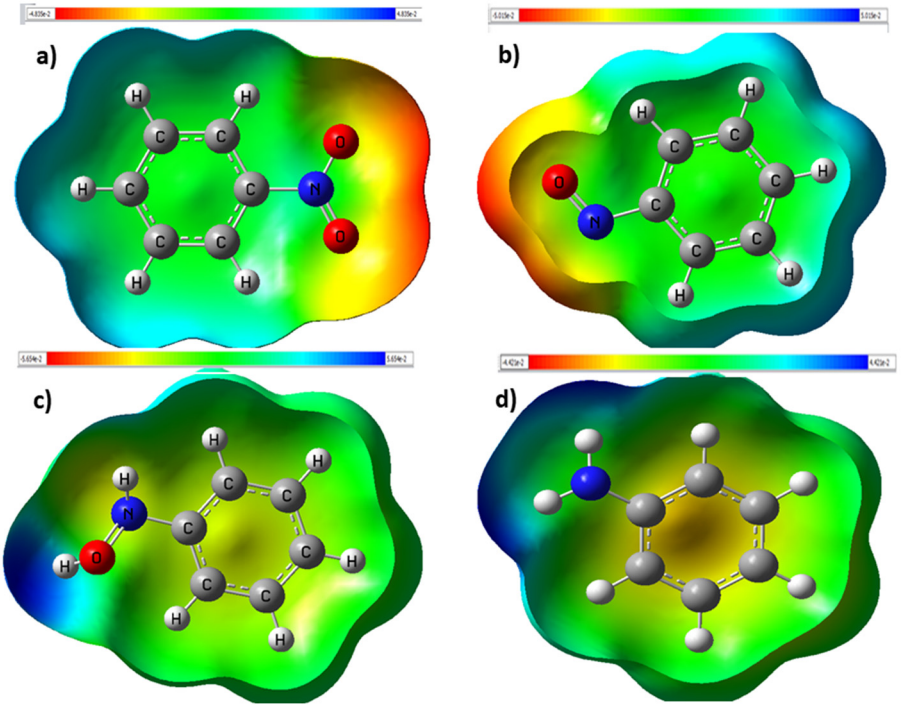

Fig. 3. ESP map gas phase a) Ph-NO_2, b) Ph-NO, c) Ph-NHOH, d) Ph-NH_2

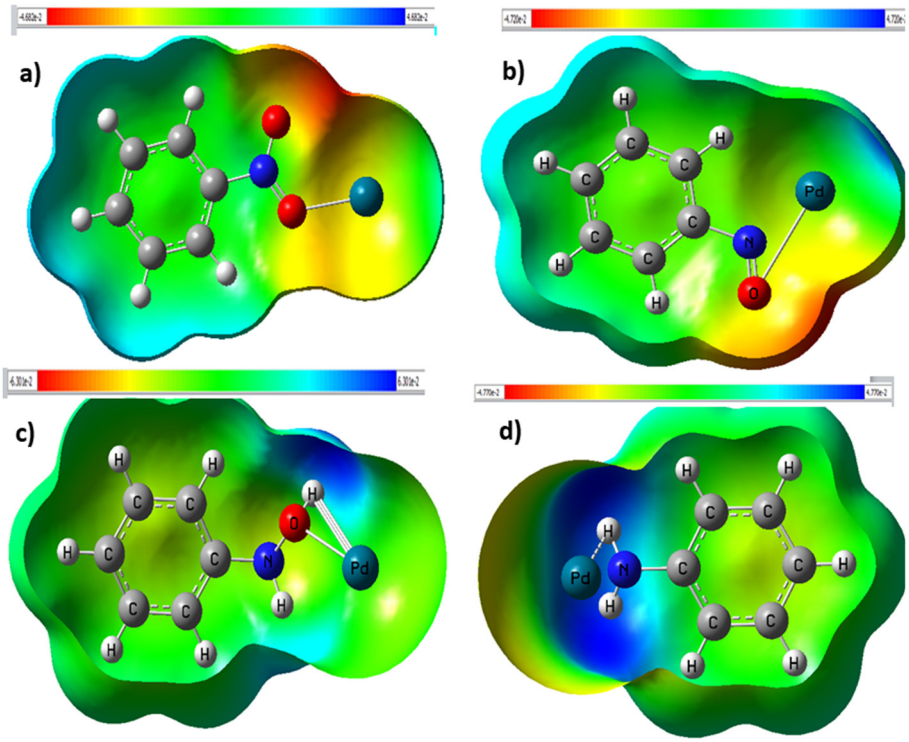

Fig. 4. ESP map (Pd surface in gas phase) a) Pd@Ph-NO_2; b) Pd@Ph-NO_2; c) Pd@Ph-NHOH; d) Pd@Ph-NH_2

3.4 Frontier Molecular Orbital (FMO) Analysis. Gap trends & reactivity (lower gap ⇒ higher reactivity). Gas-phase gaps shrink markedly from Ph-NO_2 (4.69 eV) to Ph-NO (3.25 eV), explaining why nitrosobenzene is the most electronically "soft" intermediate and readily hydrogenated next. The gap then grows again in Ph-NH_2 (5.54 eV), consistent with product stability. In ethanol, gaps compress across the board (e.g., Ph-NO_2: 1.89 eV; Ph-NO: 1.86 eV), indicating solvent-enhanced reactivity via dielectric stabilization of frontier orbitals. On Pd, the early intermediates show the smallest gaps (Pd@Ph-NO ≈ 1.73 eV; Pd@Ph-NO_2 ≈ 1.76 eV), reflecting strong metal–adsorbate coupling and back-donation that activates N–O bonds.

Gas phase:

Ph-NO_2 / Ph-NO—HOMOs span the ring and the NOx fragment; LUMOs are π* on N=O, marking the electrophilic site (your Ph-NO_2/Ph-NO images).

Ph-NHOH—HOMO density shifts toward N–OH; LUMO retains antibonding character on N–O/O–H, consistent with N–O weakening before cleavage.

Ph-NH_2—HOMO on NH_2 lone pair with ring delocalization; LUMO ring-centered → large gap, low electrophilicity, results shown in Fig. 5.

Pd-bound:

Pd@Ph-NO_2—LUMO shows Pd d/NO_2 π* mixing; HOMO spreads toward Pd → gap 1.76 eV.

Pd@Ph-NO—HOMO bridges Pd–N–O; LUMO remains Pd/NO-involved → 1.73 eV.

Pd@Ph-NHOH—both frontier orbitals involve N–O(H) with Pd contribution, matching the facilitation of N–O cleavage (ΔE 2.59 eV).

Pd@Ph-NH_2—HOMO on NH_2/Pd contact; LUMO weakly Pd-mixed; gap ~2.59 eV as the system reaches the stable product, results shown in Fig. 5.

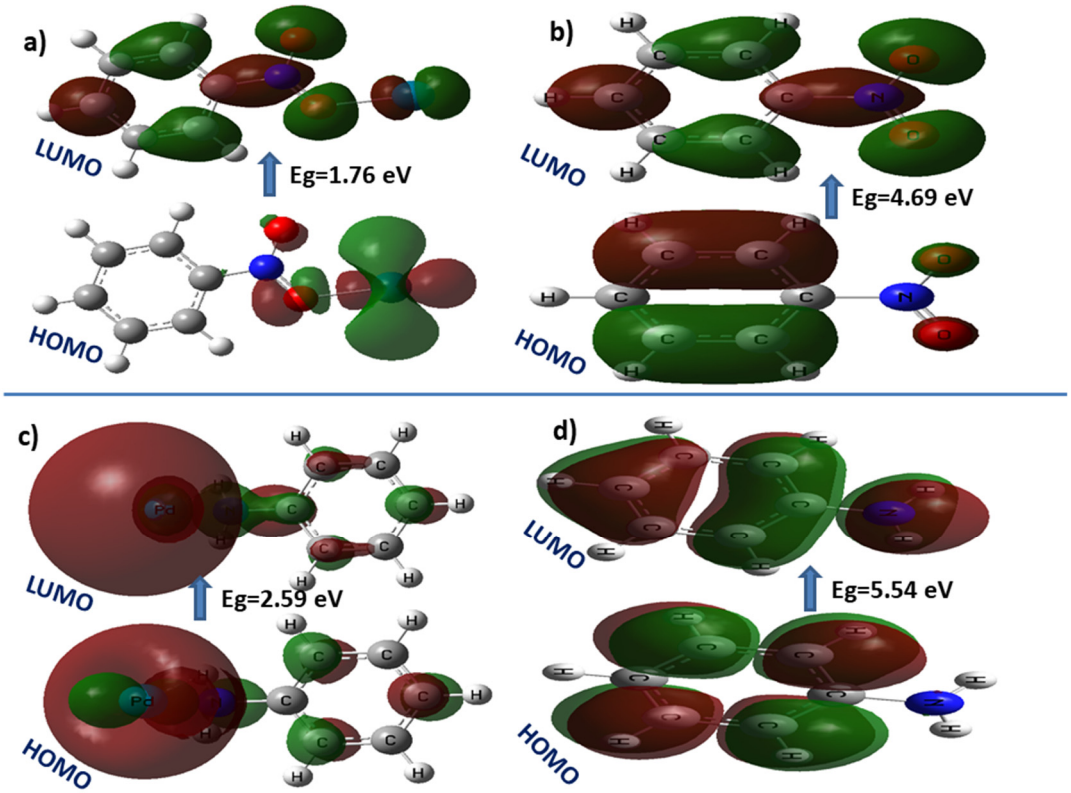

Fig. 5. (a) and (b) Gas-phase HOMO/LUMO for Ph-NO_2, and Ph-NH_2 respectively; (c) and (d) Pd-bound HOMO/LUMO for Pd@Ph-NO_2, and Pd@Ph-NH_2, respectively

3.5. IR Spectral Analysis of Intermediates and Pd Complexes. The IR spectra of the key intermediates involved in the reduction of nitrobenzene to aniline — Ph–NO_2, Ph–NO, Ph–NHOH, and Ph–NH_2 — were systematically analyzed in both the gas phase and in the presence of ethanol to evaluate solvent and catalytic effects (Fig. 6, 7 and 8). In the gas phase, Ph–NO_2 exhibited

characteristic asymmetric and symmetric NO_2 stretching vibrations at ~1530 and ~1340 cm^{-1}, respectively, while Ph–NO showed a strong N=O stretch at ~1510 cm^{-1}. Hydroxylamine (Ph–NHOH) displayed broad N–H and O–H stretches above 3300 cm^{-1}, and Ph–NH_2 was distinguished by its NH_2 stretching doublet at ~3400 cm^{-1} [32-34]. These vibrational assignments are in good agreement with literature data for substituted benzenes. Upon moving to ethanol as solvent (via PCM model), minor red shifts and broadening were observed in the OH/NH stretching regions, particularly for Ph–NHOH and Ph–NH_2, reflecting hydrogen-bonding interactions with solvent molecules (Fig. 6) [35].

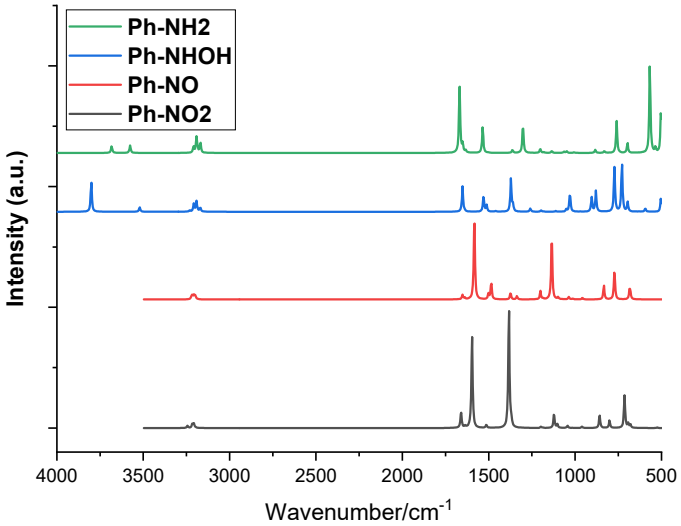

Fig. 6. Simulated IR spectra of Ph–NO_2, Ph–NO, Ph–NHOH, and Ph–NH_2 in the gas phase. (DFT FTIR: B3LYP/6-31G(d)|LANL2DZ (Gaussian 09))

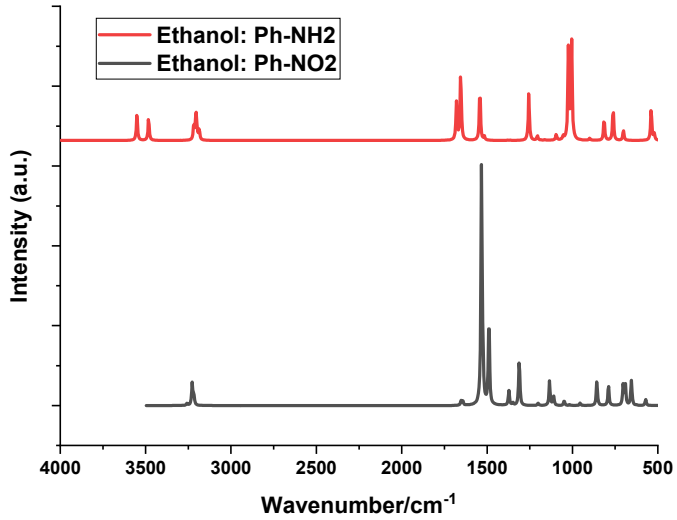

Fig. 7. Overlaid IR spectra of Ph–NO_2 and Ph–NH_2 in ethanol, showing spectral shifts due to solvent effects. (DFT FTIR: B3LYP/6-31G(d)|LANL2DZ (Gaussian 09))

In the Pd-catalyzed systems, further shifts in the IR bands indicated strong metal–ligand interactions. For example, Pd–Ph–NO_2 retained NO_2 stretching features but with slight red shifts and intensity changes (~1515 and ~1325 cm^{-1}), consistent with π-backbonding from Pd to the nitro group [36]. Similarly, Pd–Ph–NH_2 showed dampened NH_2 stretching peaks in the 3300–3400 cm^{-1} region, suggesting electronic stabilization via Pd coordination (Fig. 8). Overall, the spectral evolution across these species supports the structural and electronic transitions throughout the catalytic cycle and

validates the calculated intermediates. The clear correspondence between vibrational features and functional group changes, especially when Pd is present, supports both the mechanistic sequence and the feasibility of detection by experimental IR methods.

In the calculated FTIR spectra of Ph–NO_2 and Pd@Ph–NO_2 (Figs. 7 and 8) a weak band appears at ~3250 cm^{-1}. Since these molecules do not contain N–H or O–H groups, this feature cannot be assigned to X–H stretching vibrations of the nitro group or solvent. Normal-mode analysis shows that the corresponding vibrations involve mainly aromatic C–H stretching motions of the phenyl ring. In our harmonic DFT calculations these modes are slightly overestimated in frequency, giving rise to a band near 3250 cm^{-1}; after applying the usual scaling factor, they correspond to the experimental C–H stretching region around 3000–3100 cm^{-1}. all IR figures we notice the progressive disappearance of NO_2 bands (~1530 and ~1350 cm^{-1}) and emergence of N–H and NH_2 bands (~3300–3400 cm^{-1}) confirms the reduction sequence.

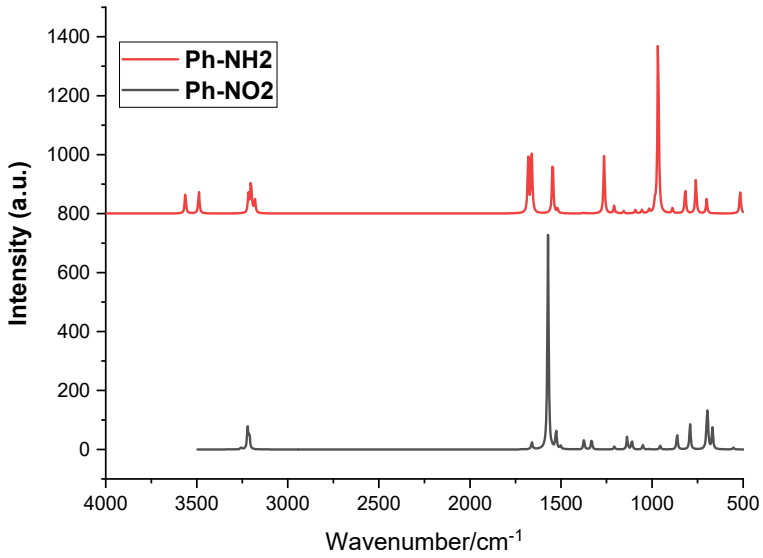

Fig. 8. IR spectra of Pd@Ph–NO_2 and Pd@Ph–NH_2 in the gas phase, highlighting metal–ligand interactions. (DFT FTIR: B3LYP/6-31G(d)|LANL2DZ (Gaussian 09))

4. Conclusion

In this work, a comprehensive DFT study was conducted to investigate the stepwise reduction of nitrobenzene to aniline via nitrosobenzene and phenylhydroxylamine intermediates. Three mechanistic environments were considered: gas phase, solvent phase (ethanol), and a palladium-catalyzed surface. Theoretical evaluations included geometry optimization, thermochemical profiling, frontier molecular orbital (FMO) analysis, and vibrational (IR) spectroscopy calculations.

The gas-phase and ethanol-solvated calculations revealed that solvation induces noticeable geometric and electronic changes across all intermediates. In ethanol, key bond lengths (e.g., N–O and N–H) were slightly elongated, and HOMO–LUMO energy gaps decreased, indicating enhanced molecular reactivity under solvated conditions. IR spectral shifts, particularly in the N=O and N–H stretching regions, further confirmed solvent-induced stabilization. In the Pd-catalyzed pathway, the adsorption of nitrobenzene and its intermediates on the Pd surface led to substantial changes in geometry and energetics. Adsorption energies confirmed favorable interactions between the molecules and the metal surface, particularly through Pd–O and Pd–N bonding. The catalytic surface effectively stabilized transition-like geometries and lowered the overall reaction energy profile, suggesting a smoother and more efficient reduction pathway compared to the uncatalyzed routes.

Overall, the findings highlight the critical influence of both solvent and metal catalyst in modulating the thermodynamics, electronic structure, and spectral behavior of the nitrobenzene reduction mechanism. These insights contribute to a deeper theoretical understanding of

hydrogenation processes and provide valuable guidance for optimizing catalytic systems in both laboratory and industrial settings.

References

1. Formenti D., Ferretti F., Scharnagl F.K., Beller M. Reduction of Nitro Compounds Using 3d-Non-Noble Metal Catalysts. *Chemical Reviews*, 2019, **Vol. 119(4)**, p. 2611-2680. DOI: 10.1021/acs.chemrev.8b00547
2. Li Z., Zhang M., Dong X., Ji S., Zhang L., Leng L., Li H., Hugh Horton J., Xu Q., Zhu J. Strong electronic interaction of indium oxide with palladium single atoms induced by quenching toward enhanced hydrogenation of nitrobenzene. *Applied Catalysis B: Environmental*, 2022, **Vol. 313**, 121462. DOI: 10.1016/j.apcatb.2022.121462
3. He W., Li Y., Xiang Q., Zhang X., Yu J., Ma Ch., Yao Y., Yin Ch., Liu Y., Zhou Y., Li X., Lu Ch. Enhancing electron penetration through carbon shell of encapsulated catalysts by Co alloying for aromatic nitrobenzene hydrogenation. *Journal of Catalysis*, 2025, **Vol. 447**, p. 116150. DOI: 10.1016/j.jcat.2025.116150
4. Serna P., Corma A. Transforming Nano Metal Nonselective Particulates into Chemoselective Catalysts for Hydrogenation of Substituted Nitrobenzenes. *ACS Catalysis*, 2015, **Vol. 5(12)**, p. 7114-7121. DOI: 10.1021/acscatal.5b01846
5. Ye T.N., Lu Y., Li J., Nakao T., Yang H., Tada T., Kitano M., Hosono H. Copper-Based Intermetallic Electride Catalyst for Chemoselective Hydrogenation Reactions. *Journal of the American Chemical Society*, 2017, **Vol. 139(47)**, p. 17089-17097. DOI: 10.1021/jacs.7b082526.
6. Lin L., Yao Y., Gao R, Liang X., Yu Q., Deng Y., Liu J., Peng M., Jiang Z., Li S., Li Y.-W., Wen X.-D., Zhou W., Ma D. A highly CO-tolerant atomically dispersed Pt catalyst for chemoselective hydrogenation. *Nature Nanotechnology*, 2019, **Vol. 14(4)**, p. 354-361. DOI: 10.1038/s41565-019-0366-5
7. Zhang S., Chang Ch.-R., Huang Z.-Q., Li J., Wu Zh., Ma Y., Zhang Z., Wang Y., Qu Y. High Catalytic Activity and Chemoselectivity of Sub-nanometric Pd Clusters on Porous Nanorods of CeO_2 for Hydrogenation of Nitroarenes. *Journal of the American Chemical Society*, 2016, **Vol. 138(8)**, p. 2629-2637. DOI: 10.1021/jacs.5b11413
8. Al-Gubury H.Y., Fairooz N.Y., Aljeboree A.M., Alqaraguly M.B., Alkaim A.F. Photcatalytic degradation n-undecane using coupled ZnO-Co_2O_3. *International Journal of Chemical Sciences*, 2015, **Vol. 13(2)**, p. 863-874.
9. Karam F.F., Kadhim M.I., Alkaim A.F. Optimal conditions for synthesis of 1, 4-naphthaquinone by photocatalytic oxidation of naphthalene in closed system reactor. *International Journal of Chemical Sciences*, 2015, **Vol. 13(2)**, p. 650-660.
10. Blaser H.-U., Steiner H., Studer M. Selective Catalytic Hydrogenation of Functionalized Nitroarenes: An Update. *ChemCatChem*, 2009, **Vol. 1(2)**, p. 210-221. DOI: 10.1002/cctc.200900129
11. Xu W., Li P., Fan J. Reduction of nitrobenzene by the catalyzed Fe/Cu process. *Journal of Environmental Sciences*, 2008, **Vol. 20(8)**, p. 915-921. DOI: 10.1016/j.jhazmat.2005.04.011
12. Niyirora P., Cyganowski P. Catalytic Production of Aromatic Amines from Nitroaromatics—Addressing a Critical Challenge in Environmental Remediation. *Chemistry – A European Journal*, 2025, **Vol. 31(24)**, e202500281. DOI: 10.1002/chem.202500281
13. Hasanova S.S. Synthesis, physicochemical study and crystal structure of bis-(p-nitrobenzoate)-di-(pyrazine) nickel(ii)-dihydrate. *Chemical Problems*, 2022, **Vol. 20(1)**, p. 95-101. DOI: 10.32737/2221-8688-2022-1-95-101
14. Mamedova L.N., Synthesis of tetrahydrated Na (I) salt of 4-carboxy 2-nitro terephthalate and its structural study. *Chemical Problems*, 2024, **Vol. 22(2)**, p. 150-156. DOI: 10.32737/2221-8688-2024-2-150-156
15. Chatterjee M., Ishizaka T., Suzuki T., Suzuki A., Kawanami H. In situ synthesized Pd nanoparticles supported on B-MCM-41: An efficient catalyst for hydrogenation of nitroaromatics

in supercritical carbon dioxide. *Green Chemistry*, 2012, **Vol. 14(12)**, p. 3415-3422. DOI: 10.1039/C2GC36160D
16. Corma A., Serna P. Chemoselective hydrogenation of nitro compounds with supported gold catalysts. *Science*, 2006, **Vol. 313(5785)**, p. 332-334. DOI: 10.1126/science.1128383
17. Chen Y., Wang C., Liu H., Qiu J., Bao X. Ag/SiO_2: A novel catalyst with high activity and selectivity for hydrogenation of chloronitrobenzenes. *Chemical Communications*, 2005, **Vol. (42)**, p. 5298-5300. DOI: 10.1039/b509595f
18. Mironenko R.M., Belskaya O.B., Likholobov V.A. Approaches to the synthesis of Pd/C catalysts with controllable activity and selectivity in hydrogenation reactions. *Catalysis Today*, 2020, **Vol. 357**, p. 152-165. DOI: 10.1016/j.cattod.2019.03.023
19. Teschner D., Révay Z., Borsodi J., Hävecker M., Knop-Gericke A., Schlögl R., Milroy D., Jackson S.D., Torres D., Sautet Ph. Understanding palladium hydrogenation catalysts: When the nature of the reactive molecule controls the nature of the catalyst active phase. *Angewandte Chemie - International Edition*, 2008, **Vol. 47(48)**, p. 9274-9278. DOI: 10.1002/anie.200802134
20. Holthausen M.C., Koch W. *A Chemist's Guide to Density Functional Theory*. 2001. p. 265-293. DOI:10.1002/3527600043
21. Sheng T., Qi Y.-J., Lin X., Hu P., Sun S.-G., Lin W.-F. Insights into the mechanism of nitrobenzene reduction to aniline over Pt catalyst and the significance of the adsorption of phenyl group on kinetics. *Chemical Engineering Journal*, 2016, **Vol. 293**, p. 337-344. DOI: 10.1016/j.cej.2016.02.066
22. Frisch M.J. *Gaussian 16 Revision C.01,*. 2016. **Vol. Gaussian Inc.,** Wallingford CT.
23. Cramer C.J., Truhlar D.G. Implicit Solvation Models: Equilibria, Structure, Spectra, and Dynamics. *Chemical Reviews*, 1999, **Vol. 99(8)**, p. 2161-2200. DOI: 10.1021/cr960149m
24. Yurdakul Ş., Tanrıbuyurdu S. Theoretical and experimental study of solvent effects on the structure, vibrational spectra, and tautomerism of 3-amino-1,2,4-triazine. *Journal of Molecular Structure*, 2013, **Vol. 1052**, p. 57-66. DOI: 10.1016/j.molstruc.2013.08.046
25. Hammer B., Norskov J.K. Why gold is the noblest of all the metals. *Nature*, 1995, **Vol. 376(6537)**, p. 238-240. DOI: 10.1038/376238a0
26. Wang H., Pu M., Lei M. Theoretical study on nitrobenzene hydrogenation to aniline catalyzed by M1/CeO_2−x(111) single-atom catalysts. *Physical Chemistry Chemical Physics*, 2025, **Vol. 27(9)**, p. 4829-4836. DOI: 10.1039/D4CP04459B
27. Ding P., Fayad E., Abu Ali O.A., Qin H.-L. A green, cheap and robust method for selective hydrogenation of nitroarenes. *Tetrahedron*, 2024, **Vol. 167**, 134269. DOI: 10.1016/j.tet.2024.134269
28. Wang X., Li Y. Chemoselective hydrogenation of functionalized nitroarenes using MOF-derived co-based catalysts. *Journal of Molecular Catalysis A: Chemical*, 2016, **Vol. 420**, p. 56-65. DOI: 10.1016/j.molcata.2016.04.008
29. Murray J.S., Politzer P. The electrostatic potential: an overview. *WIREs Computational Molecular Science*, 2011, **Vol. 1(2)**, p. 153-163. DOI: 10.1002/wcms.19
30. Suresh C.H., Remya G.S., Anjalikrishna P.K. Molecular electrostatic potential analysis: A powerful tool to interpret and predict chemical reactivity. *WIREs Computational Molecular Science*, 2022, **Vol. 12(5)**, e1601. DOI: 10.1002/wcms.1601
31. Zhang Y., Li Z., Zhang J., Xu L., Han Z.-K., Baiker A., Li G. Nanostructured Ni-MoCx: An efficient non-noble metal catalyst for the chemoselective hydrogenation of nitroaromatics. *Nano Research*, 2023, **Vol. 16(7)**, p. 8919-8928. DOI: 10.1007/s12274-023-5598-x
32. Polat T., Theoretical study of the solvent effects on the molecular structure and vibrational spectra of 2-hydroxy-4-methyl-3-nitropyridine. *Journal of Molecular Structure*, 2014, **Vol. 1067**, p. 261-270. DOI: 10.1016/j.molstruc.2014.03.017
33. Ravindranath L., Srishailam K., Reddy B.V. Experimental and DFT Quantum Chemical Studies on Structural, Vibrational and Molecular Properties of Some Substituted 4-Phenylphenols. *Polycyclic Aromatic Compounds*, 2023, **Vol. 43(10)**, p. 9233-9268. DOI: 10.1080/10406638.2022.2161584

34. Magaji B., Singh P., Skelton A.A., Martincigh B.S. A density functional theory study of a series of symmetric dibenzylideneacetone analogues as potential chemical UV-filters. *Heliyon*, 2024, **Vol. 10(21)**, e39910. DOI: 10.1016/j.heliyon.2024.e39910
35. Justin Adaikala Baskar A., Ajay Joshva L., Dhanapal D., Johnee Britto N., Jaccob M., Mansiya C., Kannappan V. Experimental and DFT investigation on the role of aromaticity on the stability of hydrogen bonded complexes of cyclohexanone with amines and hydroxyl compounds. *Journal of Molecular Liquids*, 2022, **Vol. 366**, 120221. DOI: 10.1016/j.molliq.2022.120221
36. Catellani M., Mealli C., Motti E., Paoli P., Perez-Carreño E., Pregosin P.S. Palladium−Arene Interactions in Catalytic Intermediates: An Experimental and Theoretical Investigation of the Soft Rearrangement between η1 and η2 Coordination Modes. *Journal of the American Chemical Society*, 2002, **Vol. 124(16)**, p. 4336-4346. DOI: 10.1021/ja016587e